

LONG RISE-TIME PRESSURE SIGNATURE THROUGH JET TURBULENCE IN A LABORATORY-SCALE EXPERIMENT

Takahiro Ukai*, Yuta Saito*, Ko Miyakoshi*, Takayoshi Yamaguchi*, Kiyonobu Ohtani*,
Shigeru Obayashi*

* Institute of Fluid Science, Tohoku University, Sendai, 980-8577, Japan

Keywords: *Low sonic boom, shock-turbulence interaction, laboratory-scale experiment*

Abstract

Turbulence effect on a pressure signature with the long rise time was experimentally investigated in a ballistic range facility to evaluate robustness of a low sonic boom signature. The long rise time pressure signature was produced by launching a conical projectile. High-speed schlieren photography and point-diffraction interferometer were used to visualize the density field. The pressure waveform was measured using a pressure transducer.

The turbulence effect is not critical issue for the long rise time pressure signature. The long rise time pressure signature possesses feature that the overpressure slowly increases; this is not a shock wave. A pressure wave which is not a shock wave is not affected by turbulence, although the turbulence effect appears on a shock wave possessing the short rise time.

1 Introduction

Sonic boom estimation is necessary to realize supersonic transport vehicles. The sonic boom is caused by the shock waves from a supersonic vehicle cruising at more than the speed of sound. The sonic boom produces the large noise on the ground and leads to stressful environment to human [1] therefore, significantly reducing the sonic boom is necessary. When designing a supersonic transport with a low sonic boom signature, it is extremely important to accurately estimate the sonic boom magnitude, however, this is not easy to achieve. The shock waves generated from the supersonic transport pass through the real atmosphere during reaching the

ground level, and thus the sonic boom signatures are affected by atmospheric conditions such as: turbulence, humidity, and temperature [2-4]. Although atmospheric conditions cannot be controlled, they must be considered for sonic boom estimation.

Sonic boom signature affected by turbulent effects is not easily estimated. Turbulence inside the atmospheric boundary layer has a significant effect on the sonic boom signature [5]. From the flight test results, the overpressure and the rise time which are generally defined as sonic boom characteristics are randomly varied by turbulence effects; a distorted pressure waveform possessing twice magnitude of the peak pressure level appears infrequently [6]. Lipkens *et al.* [7] have shown that in the case of shock-turbulence interaction, the mean overpressure decreases and the mean rise time increases, and the standard deviations also increase. The larger standard deviations suggest that large overpressures and short rise times may occur. Additionally, the turbulence effects are enhanced if a shock wave propagates through a turbulent field over a long distance [8]. The effects of turbulence on shock waves have been investigated [9-15], and the turbulence effect on a normal sonic boom N-shape signature might be almost understood.

The low sonic boom pressure signature does not maintain necessarily due to turbulence effects. Transmutation of a pressure waveform is useful for realization of the sonic boom reduction [16]. The pressure signature possessing the long rise time and the low overpressure leads to the sonic boom reduction.

To keep the low sonic boom pressure signature even if turbulence affects it, its characteristics by turbulence effect has to be investigated. To prove sonic boom reduction by theory, a supersonic vehicle designed by the overpressure of flat-top shape was flown in the real atmosphere [17]. The flat-top shape waveform was compared with the N-shape wave in a similar turbulence condition to evaluate effectiveness of the theory. From the flight test result, it was confirmed that turbulence effect of the low boom pressure signature was similar to the normal N-shape signature, however, we are unable to elucidate its behavior.

The turbulence effect on a low sonic boom signature can be investigated in laboratory-scale experiments. The laboratory-scale experiments are effective for investigation of the shock-turbulence interaction, because it is easy to adjust the turbulent parameters. In addition, ballistic range facilities possess ability to produce a low sonic boom signature although its waveform cannot be generated using spark generators, laser generators, or shock tubes. This is because that an arbitrarily shaped model can be launched to vary the waveform. Additionally, turbulence intensity can be easily controlled compared to supersonic wind tunnel facilities because ambient air is stationary in a test section area of ballistic ranges. Hell [18] conducted a ballistic range experiment to investigate turbulence effect on N-shape wave. The pressure characteristics affected by turbulence resembled the flight test results, however, the impinged pressure signature was N-shape because a bullet type projectile was used.

To evaluate robustness of a low sonic boom signature, its behavior by turbulence effects must be investigated. Ballistic range facilities possess ability to conduct shock-turbulence interaction experiments and are useful to investigate turbulence effects on a low sonic boom signature. In this study, turbulence effect on pressure signature with the long rise time was experimentally investigated in a ballistic range facility. In addition, we investigated turbulence effect on N-shape wave generated from a cylindrical projectile to evaluate the experimental setup. The long rise

time pressure signature was produced by launching a conical projectile. The pressure waveform was measured using a pressure transducer. The distorted shock wave was visualized using high-speed schlieren photography and point-diffraction interferometer.

2 Experimental setup

2.1 Ballistic range facility

An effect of turbulence on a pressure signature with the long rise time was investigated experimentally. To generate the pressure signature with long rise time, a ballistic range, which is a single-stage powder gun mode, at the Institute of Fluid Science, Tohoku University was used. The ballistic range consists of a propellant chamber, a launch tube 15 mm in inner diameter, and a recovery tank 1.66 m in inner diameter and 12 m in length. A projectile is accelerated by igniting a rifle cartridge (Winchester 300) filled with a smokeless powder (HS-7 Hodgdon Powder Co.). A blast tube was connected at the launch tube end, making it effective to attenuate a precursory blast wave driven in front of the projectile. An experimental setup in the recovery tank is illustrated in Fig. 1. A projectile flies from left side to right side. When the projectile ran through the blast tube, its passing timing was captured by cutting off a laser beam, and this signal was used as a trigger signal for the measurements. The launched projectile was stopped at the catch tank after measuring the pressure waveform and visualizing the shock wave.

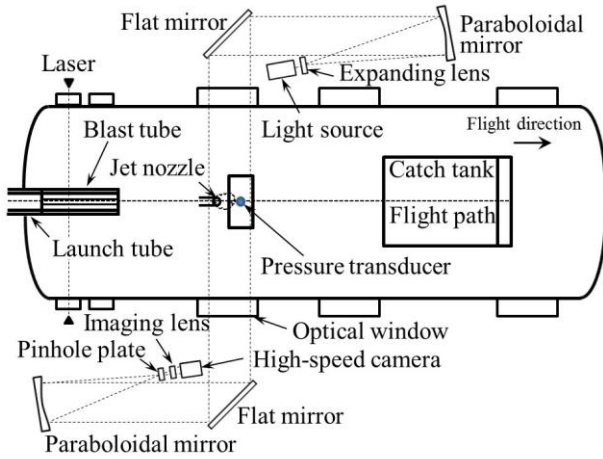


Fig. 1. The experimental setup.

2.2 Projectiles

Figure 2 shows the cylindrical and conical projectiles. The cylindrical projectile 15 mm in diameter and 70 mm in length was made of polyamide resin 15 g in mass [Fig. 2 (a)] and generates a pressure waveform with N-shape during the launching in supersonic. This projectile is useful to visualize a distorted shock wave because of strong density change around it. The low sonic boom signature with the long rise time was obtained by launching the conical projectile 15 mm in diameter and 163 mm in length [Fig. 2 (b)]. Carlson *et al.* [19] defined the dimension of this conical projectile, its near-field pressure waveform possesses the low overpressure and the long rise time. The projectile 25 g in mass consisted of different materials which are polyamide resin and steel. The steel part prevents the deformation of the nose by aerodynamic force, however, we did not use steel material at contact surface to the launch tube to avoid damage of the launch tube. The launching projectile velocity was set at a Mach number of 1.5 and 1.4 in this experiment.

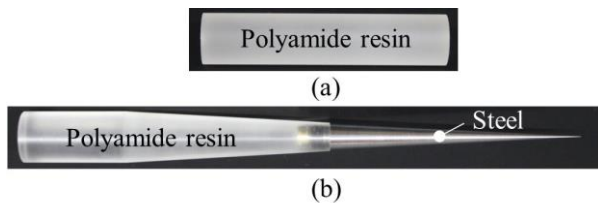


Fig. 2. The cylindrical and conical projectiles.

2.3 Near-field pressure measurement

The near-field pressure measurement system is shown in Fig. 3. The pressure waveform was measured using a flash-mounted piezoelectric pressure transducer (PCB Piezotronics, inc. model: 113B28, rise time: under 1 μ s, resolution: 7 Pa, resonant frequency: over 500 kHz) in an acrylic plate, which 96 mm \times 200 mm \times 30 mm (length \times width \times thickness) in size, was located at approximately 1300 mm long from the blast tube end. To prevent an effect of a mechanical oscillation on the pressure waveform, the pressure transducer was screwed to a mount holder made of MC nylon. The acrylic plate with the pressure transducer was positioned at 140 mm height under the flight path, and its angle was adjusted so that the shock wave front surface contacts with the pressure transducer. The pressure signals was recorded using a digital oscilloscope (Yokogawa Electric Corp., model: DL750) via a signal conditioner with low noise (PCB Piezotronics, Inc. model: 482A22). 10 MS/s was set as the sampling rate in order to accurately measure the pressure waveform.

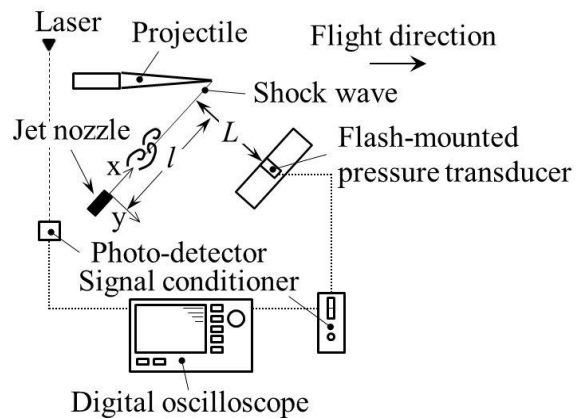


Fig. 3. The near-field pressure measurement system.

2.4 Turbulence impingement

The shock wave interacted with a turbulent field generated by a circular jet nozzle 4.5 mm in inner diameter. The jet impingement condition was different between the cylindrical projectile and the conical one (Table 1). High pressure dry air supplied through a pressure regulator and a flexible tube was used as the jet gas. To control

the jet velocity, the static pressure at the nozzle end was kept at 60 kPa.

To evaluate the turbulent field, a hot-wire anemometer (Institute of Flow Research Corp., model: CTA-002) with an X-probe (KANOMAX Corp., model: 0252R-T5) was used. The voltage signals from the hot-wire anemometer were recorded by the same Yokogawa oscilloscope at a sampling rate of 100 kHz with a recording time of 2 seconds. The voltage signals were calibrated before the turbulent measurement. A pitot tube anemometer connected to a digital manometer (COSMO Instrument Co., Ltd, model: DM-3501) was located next to the hot-wire anemometer for calibration, and the mean velocity was measured using the pitot tube as a reference. The voltage signals from the digital manometer was recorded using a compact DAQ system (National Instruments Corp., model: 9205) driven by LabVIEW 2011. When the turbulent field was evaluated, the pitot tube and pressure transducer were removed.

Table 1 The jet impingement condition.
l: Jet impinging location from the jet nozzle.
L: Impinging shock propagation distance.

	Cylindrical projectile	Conical projectile
<i>l</i>	112 mm	102 mm
<i>L</i>	61 mm	40 mm

2.5 Flow visualization

The high-speed schlieren photography and the point-diffraction interferometer (PDI) were employed to visualize a distorted shock wave by impinging the turbulence. The unsteady flow visualization using PDI system has been successfully applied in past studies [20]. The optical arrangement became tricky due to limited space around the facility (see Fig. 1). A pair of 300 mm diameter parabolic mirrors with 2800 mm focal length and a pair of 550 mm diameter flat mirror were used. A light supplied from a continuous cw green laser (Coherent Inc., model: COMPASS 315M-50, wavelength = 532 nm, output power = 50 mW). The laser beam expanded by an expanding lens was collimated by the parabolic mirror and changes the

direction by the flat mirror. The collimated light passes through the test section via the optical glass windows and then was reflected by the second flat mirror and parabolic mirror. The offset angle between the collimated light beam and light source was same degree to prevent coma. To obtain an interferogram, a small pinhole which is constructed on a semi-transparent plate was located at laser focus point of the second parabolic mirror. A converging light is diffracted when passing through the pinhole and spreading semi-spherically. This diffracted light acts as a reference beam and overlapped with the object beam, making it possible to form an interference pattern [21, 22]. A knife edge horizontally positioned was used in the schlieren photography mode as a substitute for the pine hole. Visualization images were recorded by using a high-speed digital video camera (Shimadzu Corp., model: HPV-X, 128 frames at 400 × 250 pixels spatial resolution). A frame rate of 200 kfps with an exposure time of 1 μs was used.

3 Results and discussion

3.1 Turbulent characteristics

Figure 4 shows the distribution of the turbulence intensity V_{rms}/U_{mean} of the y component in the x-y plane, measured using the hot-wire technique. The right-handed coordinate system is employed (see Fig. 3). The turbulence intensity is defined as the root mean square velocity of a component divided by its mean velocity. In this paper, only the turbulence intensity of the y component was described because turbulence intensity which is same direction as shock propagation direction strongly affects a pressure waveform [23, 24]. The almost symmetric turbulent field was generated in this experiment. Figure 5 shows the mean velocity U_{mean} in the x-y plane. At coordinate ($x = 102$, $y = 0$, $z = 0$), the mean velocity of the x component was $U_{mean} = 88.3$ m/s. A Reynolds number of 2.6×10^4 based on the jet nozzle inner diameter was obtained.

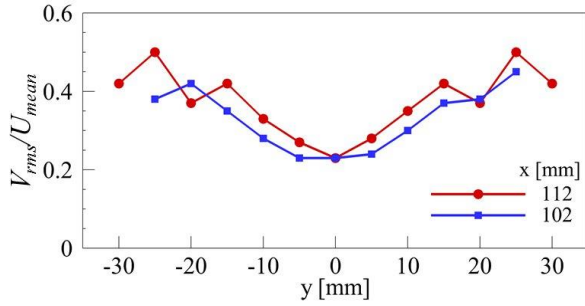


Fig. 4. Distributions of the turbulence intensity of the y component.

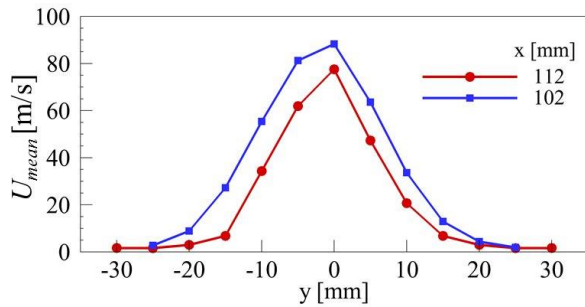


Fig. 5. Distributions of the mean velocity of the x component.

3.2 Shock-turbulence interaction

3.2.1 Pressure signature with N-shape

Figure 6 shows an instantaneous schlieren image of the cylindrical projectile. A shock wave front of a bow shock impinged to the pressure transducer locating it in parallel. A shock wave generated behind the front edge of the projectile is defined as a secondary shock in this paper. A recompressed shock was observed behind the projectile. Launching the three projectiles, the pressure waveform passed through the turbulent field was measured and compared to the two waveforms without shock-turbulence interaction.

The shock wave front was disturbed when it passes through the turbulent field. The sequential PDI visualization images with and without shock-turbulence interaction are shown in Fig. 7. In the case of shock-turbulence interaction [Fig. 7 (a)-(f)], the distortion bow shock wave front was observed [Fig. 7 (a)], and then the distance between each interference pattern which denotes isopycnic line varied with time [Fig. 7 (b), (c), and (d)]. After the shock front passed through the strong turbulent field, this distance became wide by diffusing the deformation [Fig. 7 (e) and (f)]. On the other

hand, the density contour was almost uniform when the turbulence did not imping on the shock waves.

Figures 8 and 9 show typical N-shape waveforms without and with shock-turbulence interaction, respectively. These waveforms were processed by a digital low-pass filter which is the cutoff frequency of 300 kHz because the oscillating signals occurred by resonant frequency of the pressure transducer. This digital low-pass filter with FIR (finite impulse filter) type was designed by using MATLAB R2013a. The gain value of the low-pass filter possess flat characteristic during a pass frequency. The pressure which denotes the primary peak is rose by the bow shock. The secondary shock leads to the pressure recovery from the compression pressure field to the ambient pressure. The recompressed shock possesses the same capability as the secondary shock.

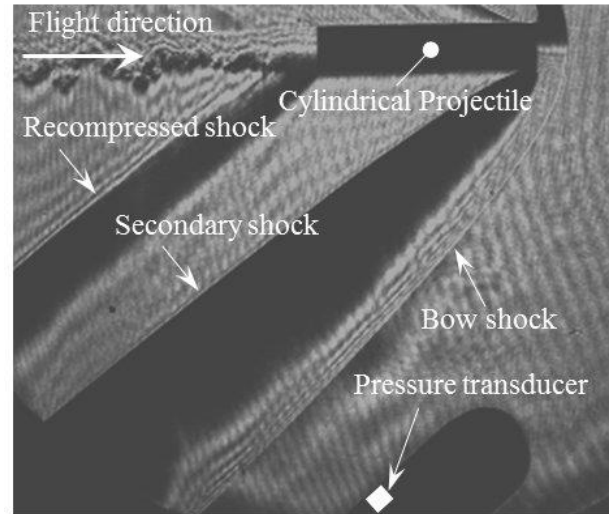


Fig. 6. Schlieren image of the cylindrical projectile (without shock-turbulence interaction, $M = 1.50$).

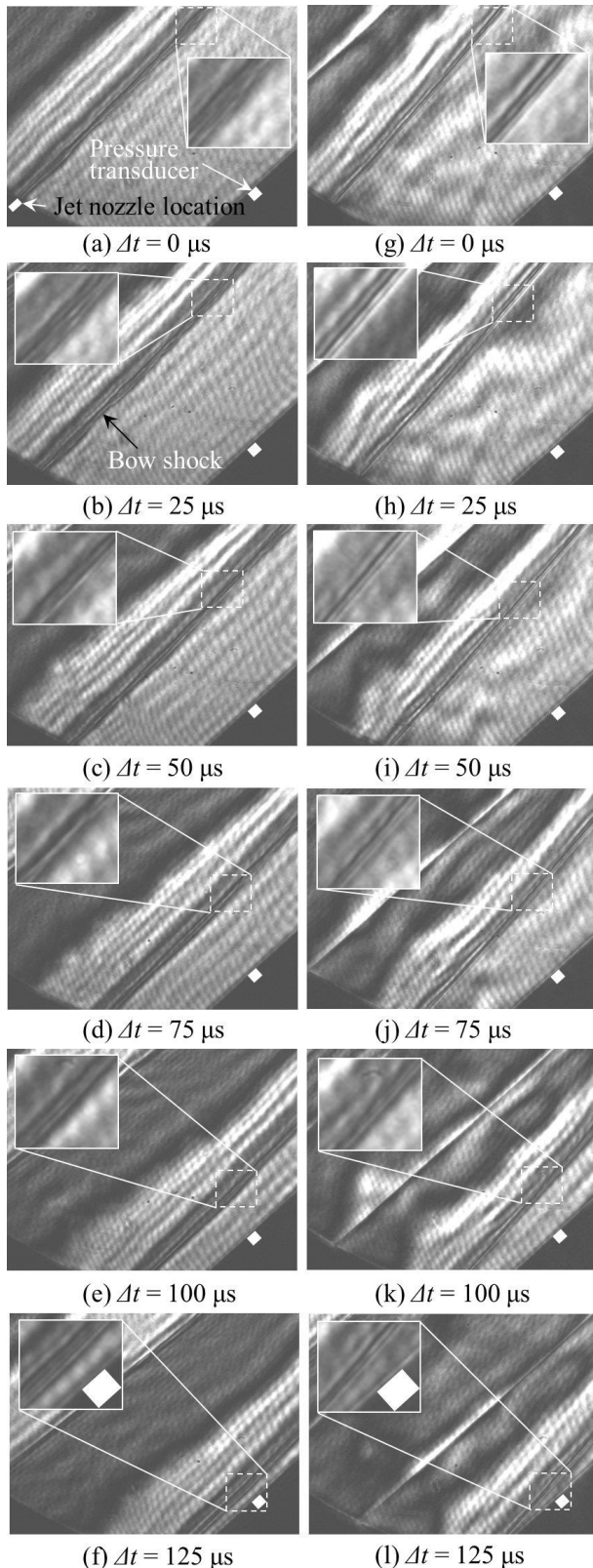


Fig. 7. Sequential PDI visualization images; the left (a-f) and right (g-l) images show with and without shock-turbulence interaction, respectively.

The short rise time pressure signature was strongly affected by turbulence interaction. When the shock wave passed through the turbulent field, the peak shape of the overpressure (circular dotted line) transmuted into either round or spike shape, compared to the N-shape waveform without shock-turbulence interaction. Although the statistics value was not evaluated due to small number of projectiles, this behavior resembled it seen in Lipkens experimental result [7] which corresponded to flight test results. Hence, this experimental setup can evaluate shock-turbulence interaction in the laboratory-scale experiment.

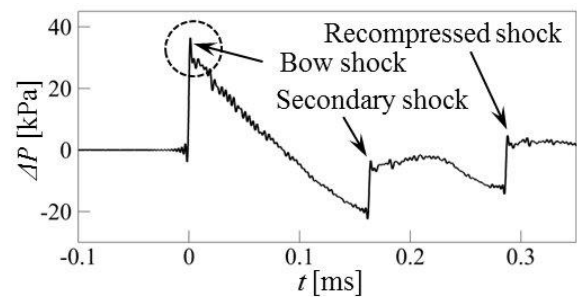
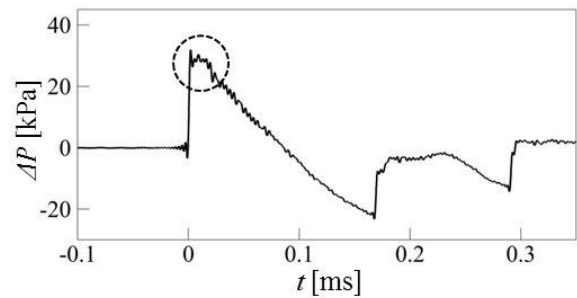
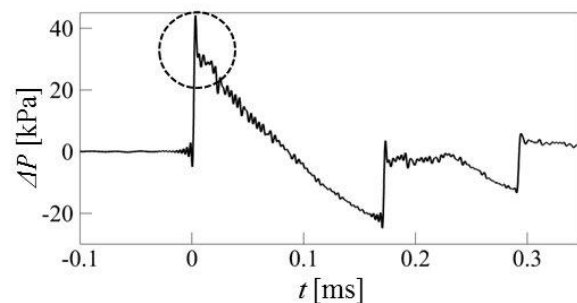


Fig. 8. Typical N-shape waveform without shock-turbulence interaction.



(a) Round peak shape waveform



(b) Spike peak shape waveform

Fig. 9. Typical N-shape wave with shock-turbulence interaction.

3.2.2 Pressure signature with the long rise time

The schlieren image of the density field around the conical projectile is shown in Fig. 10. A primary shock was generated from the nose of the projectile. The long rise time was induced by the pressure waves generated from the conical part; the pressure with long rise time was generated by the pressure field between the primary shock and the expansion shock. The gap shocks were generated from the connection part between the materials which are polyamide resin and steel. This is because the gap appeared between them due to the transmutation of the projectile by the gravity or aerodynamic force although the projectile surface was smooth around this connection. We launched ten projectiles (4 shots: without shock-turbulence interaction, 6 shots: with shock-turbulence interaction) to investigate the turbulence effect on the long rise time pressure signature.

The turbulence effect was not critical issue for the long rise time pressure signature. Figure 11 shows the sequential schlieren visualization images. Image processing driven by MATLAB R2013a was conducted to clearly observe the shock waves. In the case of the shock-turbulence interaction, the gap shock wave front was distorted by turbulence effect [Fig. 11 (d)] although a distorted primary shock wave was not observed. This is because the primary shock is weak pressure change compared with the gap shocks, therefore it is difficult to visualize its distortion even if the shock wave is affected by the turbulence. The measured pressure waveforms are shown in Fig. 12. For without shock-turbulence interaction [Fig. 12 (a)], the primary shock and the gap shocks possess the short rise time: the overpressure rapidly increases. When the shock waves passed through the turbulent field, the rise time of the primary shock increased [Fig. 12 (b)], and the pressure waveform generated from the gap shocks was also affected because the peaks became round shape. However, the long rise time location, which is defined as the pressure distribution during the time of approximately 0 - 0.23 ms, was hardly observed; the pressure field between the primary shock and the gap shocks might be not affected by turbulence. It seems that the long rise time pressure signature, which

is not a shock wave, is not affected by turbulence although turbulence affects the short rise time pressure signature.

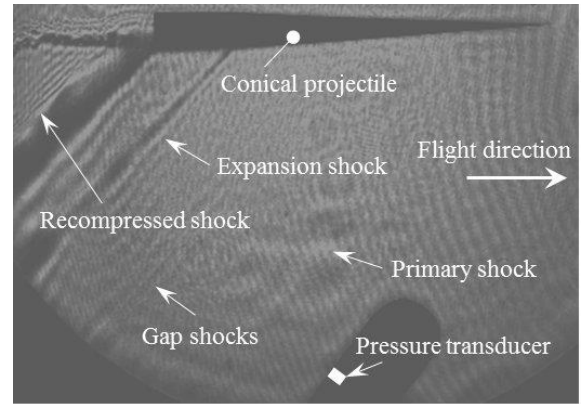


Fig. 10. Schlieren image of the conical projectile (without shock-turbulence interaction, $M = 1.35$).

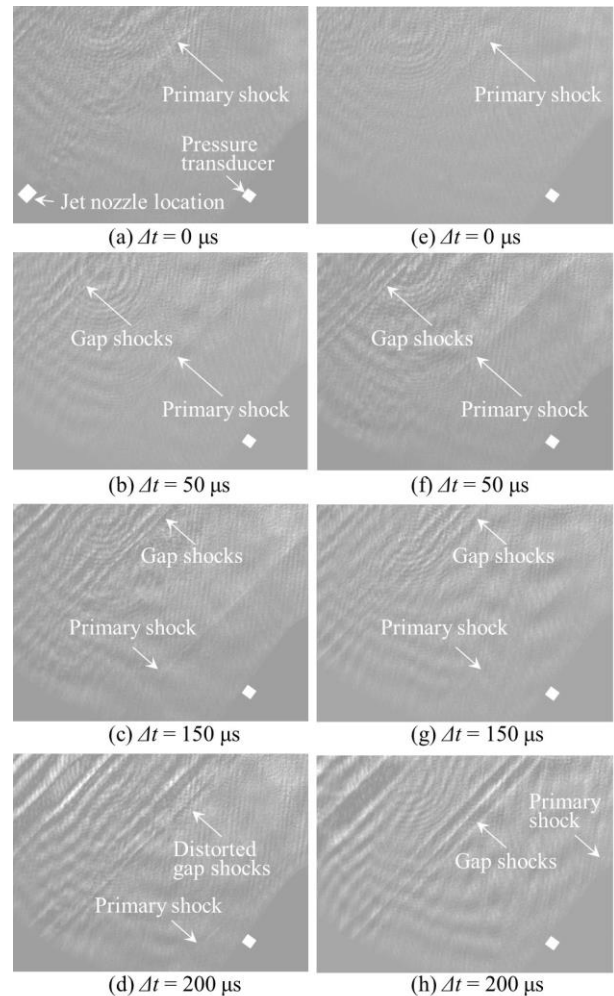
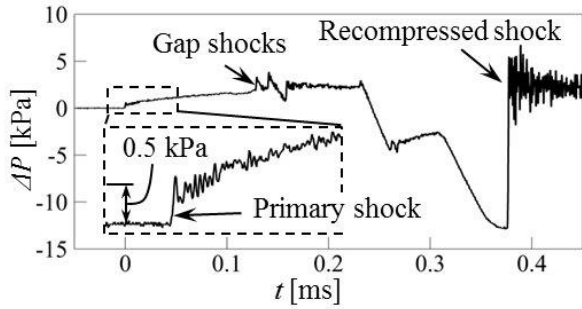
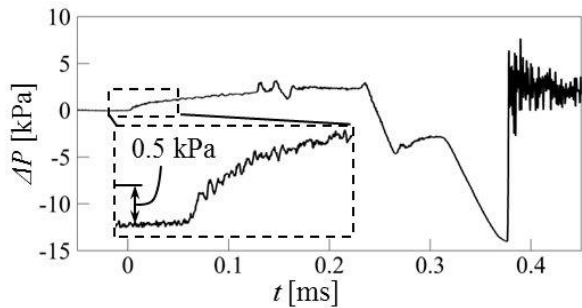


Fig. 11. Processed sequential schlieren visualization images; the left (a-d) and right (e-h) images show with and without shock-turbulence interaction, respectively.



(a) Without shock-turbulence interaction



(b) With shock-turbulence interaction
 Fig. 12. Typical pressure waveform.

4 Conclusion

Turbulence effect on a pressure signature with the long rise time was experimentally investigated in a ballistic range facility. In addition, we investigated turbulence effect on N-shape wave generated from a cylindrical projectile to evaluate the experimental setup. The long rise time pressure signature was produced by launching a conical projectile. High-speed schlieren photography and point-diffraction interferometer were used to visualize the density field. The pressure waveform was measured using a pressure transducer.

Shock-turbulence interaction can be sufficiently evaluated in this experimental setup. This is because the general behavior of turbulence effect was observed from the experimental results of the N-shape pressure waveform interacting with turbulent field. The peak shape of the overpressure transmuted into either round or spike shape, compared to the N-shape waveform without shock-turbulence interaction. In addition, the distorted shock wave front by turbulence effect was observed.

The turbulence effect was not critical issue for the long rise time pressure signature. The long rise time pressure signature possesses

feature that the overpressure slowly increases; this is not a shock wave. A pressure wave which is not a shock wave was not affected by turbulence, although the turbulence effect on a shock wave possessing the short rise time was observed.

Acknowledgment

The authors are indebted to the technical staff of the Institute of fluid science, Tohoku University, especially to Mr. Toshihiro Ogawa for the operation of the ballistic range and appreciate Mr. Masataka Honna and Mr. Hidenori Ojima for manufacture.

References

- [1] Ragnar R, Stefan S, Kenneth B and Carina B. Experiments on the Effect of Sonic - Boom Exposure on Humans. *J. Acoust. Soc. Am.*, Vol. 51, No. 2, pp 790-798, 1972.
- [2] Hodgson, P J. Vibrational relaxation effects in weak shock waves in air and the structure of sonic bangs. *J Fluid Mechanics*, Vol. 58, Part 1, pp 187-196, 1973.
- [3] Hatanaka K and Saito T. Numerical analysis of weak shock attenuation resulting from molecular vibrational relaxation. *Shock waves*, Vol. 21, pp 121-129, 2011.
- [4] Vuldashev V P, Averiyarov V M, Khokhlova A V, Ollivier S and Blanc-Benon Ph. Nonlinear Spherical Divergent Shock Waves Propagating in a Relaxing Medium. *Acoustical Physics*, Vol. 54, No. 1, pp 40-50, 2008.
- [5] Kane E J. Some effect of the atmosphere on sonic boom. *Proceedings of Sonic Boom Research*, NASA SP-147, pp 49-63, 1967.
- [6] Hilton D A, Huckel V and Maglieri D J. Sonic-boom measurements during bomber training operations in the Chicago area. NASA Technical Note, NASA TN D-3655, 1966.
- [7] Lipkens B and Blackstock D T. Model experiment to study sonic boom propagation through turbulence. Part I: General results. *J. Acoust. Soc. Am.*, Vol. 103 No. 1, pp 148-158, 1998.
- [8] Lipkens B and Blackstock D T. Model experiment to study sonic boom propagation through turbulence. Part II. Effect of turbulence intensity and propagation distance through turbulence. *J. Acoust. Soc. Am.*, Vol. 104 No. 3, pp 1301-1309, 1998.
- [9] Lipkens B. Model experiment to study sonic boom propagation through turbulence. Part III: Validation of sonic boom propagation models. *J. Acoust. Soc. Am.*, Vol. 111 No. 2, pp 509-519, 2002.

- [10] Ribner H S, Morris P J and Chu W H. Laboratory simulation of development of superbooms by atmospheric turbulence. *J. Acoust. Soc. Am.*, Vol. 53 No. 3, pp 926-928, 1973.
- [11] Harasaki T, Kitamura T, Sasoh A, Nagata K and Sakai Y. Two-point measurements of post-shock overpressure past a grid turbulence. *Proceedings of the 29th International Symposium on Shock Waves, USA*, conference paper 0246-000074, 2013.
- [12] Kim J H, Sasoh A and Matsuda A. Modulations of a weak shock wave through a turbulent slit jet. *Shock Waves*, Vol. 20, pp 339-345, 2010.
- [13] Niedzwiecki A and Ribner H S. Subjective loudness of N-wave sonic booms. *J. Acoust. Soc. Am.*, Vol. 64 No. 6, pp 1617-1621, 1978.
- [14] Pierce A D. Statistical theory of atmospheric turbulence effects on sonic-boom rise times. *J. Acoust. Soc. Am.*, Vol. 49 No. 3, pp 906-924, 1971.
- [15] Averkiou M A and Cleveland R O. Modeling of an electrohydraulic lithotripter with the KZK equation. *J. Acoust. Soc. Am.*, Vol. 106 No. 1, pp 102-112, 1999.
- [16] Seebass R and George A R. Sonic-Boom Minimization. *J. Acoust. Soc. Am.*, Vol. 51, No. 2, Part 3, pp 686-694, 1972.
- [17] Morgenstren M J, Arslan A, Lyman V and Vadyak J. F-5 Shaped Sonic Boom Demonstrator's Persistence of Boom Shaping Reduction through Turbulence. *Proceedings of 43rd AIAA Aerospace Sciences Meeting and Exhibit, USA*, AIAA paper 2005-12, 2005.
- [18] Hall S V. Distortion of the sonic-boom pressure signature by high-speed jets. *J. Acoust. Soc. Am.*, Vol. 63 No. 6, pp 1749-1752, 1978.
- [19] Carlson H W. An Investigation of the influence of lift on sonic-boom intensity by means of wind-tunnel measurements of the pressure fields of several wing-body combinations at a Mach number of 2.01. NASA TN D-881, 1961.
- [20] Numata D and Ohtani K. Application of a point-diffraction interferometer to unsteady shock wave phenomena. *Proceedings of 15th International Symposium on Flow Visualization, Belarus*, 2012.
- [21] Smartt R N and Strong J. Point-Diffraction Interferometer. *J. Opt. Soc. Am.*, Vol. 62, pp 737, 1972.
- [22] Smartt R N and Steel W H. Theory and application of point-diffraction interferometers. *Jpn. J. Appl. Phys.*, Vol. 14, Suppl. 14-1, pp 351-356, 1974.
- [23] Averianov M, Blanc-Benon Ph, Cleveland R O and Khokhlova V. Nonlinear and diffraction effects in propagation of N-waves in randomly inhomogeneous moving media. *J. Acoust. Soc. Am.*, Vol. 129, pp 1760-1772, 2011.
- [24] Aver'yanov M V, Khokhlova V A, Sapozhnikov O A, Blanc-Benon Ph and Cleveland R O. Parabolic equation for nonlinear acoustic wave propagation in inhomogeneous moving media. *Acoust. Phys.* Vol. 52, pp 623-632, 2006.

Copyright Statement

The authors confirm that they, and/or their company or organization, hold copyright on all of the original material included in this paper. The authors also confirm that they have obtained permission, from the copyright holder of any third party material included in this paper, to publish it as part of their paper. The authors confirm that they give permission, or have obtained permission from the copyright holder of this paper, for the publication and distribution of this paper as part of the ICAS 2014 proceedings or as individual off-prints from the proceedings.